Multifrequency ESR in $ET_2MnCu[N(CN)_2]_4$: A radical cation salt with quasi-two-dimensional magnetic layers in a three-dimensional polymeric structure

K. L. Nagy,[1,*] B. Náfrádi,[2,3] N. D. Kushch,[4] E. B. Yagubskii,[4] E. Herdtweck,[5] T. Fehér,[1] L. F. Kiss,[6] L. Forró,[2] and A. Jánossy[1]

[1]*Department of Experimental Physics and Condensed Matter Research Group of the Hungarian Academy of Sciences, Budapest University of Technology and Economics, P.O. Box 91, H-1521 Budapest, Hungary*

[2]*Institute of Physics of Complex Matter, EPFL, CH-1015 Lausanne, Switzerland*

[3]*Max Planck Institute for Solid State Research, Heisenbergstrasse 1, D-70569 Stuttgart, Germany*

[4]*Institute of Problems of Chemical Physics, RAS, Chernogolovka, Moscow Region 142432, Russia*

[5]*Technische Universität München, Lichtenberg Str. 4, 85747 Garching, Germany*

[6]*Research Institute for Solid State Physics and Optics, P.O. Box 49, H-1525 Budapest, Hungary*

(Received 24 April 2009; revised manuscript received 24 July 2009; published 9 September 2009)

The radical cation salt, $ET_2MnCu[N(CN)_2]_4$, [ET=bis(ethylenedithio)tetrathiafulvalene] with an unusual three-dimensional anionic polymeric network is studied by x-ray diffraction, static susceptibility measurements, and electron spin resonance (ESR) at frequencies between 9 and 420 GHz. The magnetic properties are determined by the alternating two-dimensional layers of the Mn^{2+} ions of the network and the partially charged ET molecules. At ambient temperature the overlap between Mn^{2+} ions and ET molecules is weak and an exchange integral $|J_{Mn-ET}| \approx 4 \cdot 10^{-2}$ K is estimated from their resolved ESR lines. At lower temperatures, $ET_2MnCu[N(CN)_2]_4$ is not a simple system of weakly interacting paramagnetic ions in spite of the isotropic, Curie-like static susceptibility. There are first-order phase transitions at 292 K and in the range of 120–180 K. One of the lattice constants shows anomalous temperature dependence below 292 K. Anisotropic ESR shifts appear below 150 K, which we explain by demagnetizing fields of the platelike crystals and an exchange-narrowed fine structure. The latter contributes significantly to the shift when the populations of Zeeman levels are altered in high magnetic fields at low temperatures. We estimated the exchange coupling between Mn^{2+} ions within a layer, $J_{Mn\text{-}Mn} \approx -48$ K and determined the fine structure parameters below 150 K, showing a distortion in the plane of the Mn^{2+} ions.

DOI: 10.1103/PhysRevB.80.104407 PACS number(s): 75.30.Et, 76.30.Fc, 61.66.−f

I. INTRODUCTION

The synthesis of magnetic molecular conductors is a flourishing field of material science.[1] Layered molecular materials where physical properties are tuned by modifying the widely different molecular constituents are one of the most promising approaches. A common scheme is to form a charge transfer salt with alternating layers of TTF-derivative cations (TTF=tetrathiafulvalene) and transition metal complex anions. The narrow band of overlapping chalcogen π orbitals that protrude from the planar TTF-derivative molecules is sensitive to fine details of the anion layers. The π-electrons are confined to the two-dimensional (2D) layers formed by the cations. The overlap between the π-electron band and electrons in the neighboring anionic layers is usually weak.

One of the current challenges in the field is to understand how the coupling between the magnetic *d* electrons of the anions and the delocalized π-electron band of the cations leads to the diverse ground states observed. For example, in the family of the quarter filled β-ET_2X compounds [ET =bis(ethylenedithio)tetrathiafulvalene] the ground state of the unpaired radical cation electrons can be an antiferromagnetic insulator, a superconductor, or a metal[2] depending on fine details of the interaction between the anion layers and the molecular arrangement of the ET layers. Some compounds in this class of materials are rather exotic, e.g., coexistence of ferromagnetic order and metallic conductivity was found in β-$ET_{2.7}MnCr(C_2O_4)_3$, a system of alternating insulating magnetic two-dimensional polymeric layers of bimetal oxalate anions and conducting ET molecular layers.[3]

The recently synthesized radical cation salt, $ET_2MnCu[N(CN)_2]_4$,[4] investigated in this paper differs from the above mentioned materials in that a three-dimensional (3D) polymeric anion network encages the ET molecules (Fig. 1). In spite of the 3D anion network, the magnetic structure is quasi-2D and there are well separated layers of interacting octahedrally coordinated Mn^{2+} ions and semiconducting layers of ET radical cations. In the present high field electron spin resonance (ESR) study we show that this material has an interesting magnetic structure with at least two phase transitions in the temperature range from room temperature to 100 K. The ESR lines of the manganese ions and ET molecules are resolved above 150 K in high magnetic fields. The observation of resolved ESR lines of the cationic molecular layers and magnetic ions in the neighboring anionic layers[5,6] is an indication of an extremely weak overlap. In a typical experiment, the ESR lines are resolved if the exchange energy between these layers is of the order of or less than 10^{-6} eV. On the other hand, 2D magnetic interactions within the Mn layers are strong and give rise to large anisotropic ESR shifts below 150 K. However, as the interactions between layers are weak, no 3D magnetic order is reached down to 1.8 K and the static susceptibility is almost isotropic at all temperatures.

The paper is organized as follows. Section II describes sample growth and the instruments used in this study. The

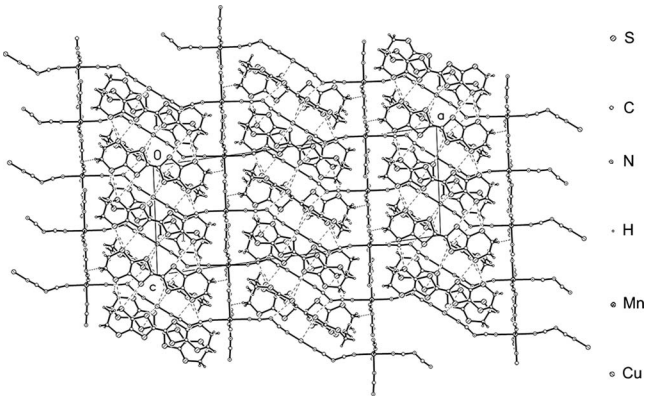

FIG. 1. Layers of ET molecules interpenetrated by the 3D polymeric anion network. Projection of the structure on the (a,c) plane.

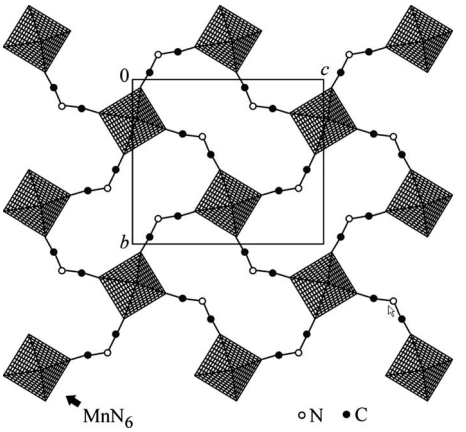

FIG. 2. Octahedrally coordinated manganese ions connected by dicyanamid (dca) ligands in the (b,c) plane. Magnetic properties arise mostly from the manganese ions.

crystal structure including x-ray data is described in Sec. III. Magnetic measurements are detailed in Sec. IV: static magnetization data in Sec. IV A and ESR data in Secs. IV B and IV C. Section IV B discusses ESR data above 120 K where at high magnetic fields the ET and Mn resonances are resolved. Sec. IV C details the low temperature data and shows that large anisotropic shifts imply a structural distortion in the (b,c) plane that is absent at high temperature. Conclusions are drawn in Sec. V.

II. EXPERIMENTAL

Single crystals of $ET_2MnCu[N(CN)_2]_4$ were grown by the electrochemical method described elsewhere.[4] The crystals are diamond shaped shiny black platelets with typical dimensions of $0.7\times0.7\times0.07$ mm^3. According to x-ray measurements the longer and shorter diagonals of the diamond coincide with the b and c axes of the crystal, respectively. We denote the direction perpendicular to the (b,c) plane by a^*. We used the morphology to orient the crystals for the ESR and superconducting quantum interference device (SQUID) magnetization measurements. The deviation between the a and a^* directions is small (6°) and we refer to g factor and susceptibility measurements along a^* as along a "main axis".

X-ray crystallographic data were collected using the same crystal as in a previous work[4] on a Bruker Smart diffractometer with graphite-monochromated MoK α radiation (λ =0.71073 Å) in an ω-scan mode. The structure was solved by direct methods and successive Fourier difference synthesis using SHELXS-97 (Ref. 7) and SHELXL-97 (Ref. 8) programs. The refinement was done by the full matrix least-squares method in an anisotropic approximation for all non-hydrogen atoms using the SHELXL-97 (Ref. 8) program. All hydrogen atoms were placed in geometrically calculated positions. Corrections for x-ray absorption were performed.

Static magnetization was measured on a single crystal with a Quantum Design MPMS-5S SQUID magnetometer between 1.8 and 300 K and magnetic fields up to 5 T.

Three electron spin resonance spectrometers were used: home built spectrometers at 75, 150, 222.4, and 225 GHz in Budapest, and at 210, 315, and 420 GHz in Lausanne, and a commercial Bruker ELEXSYS 500 at 9.4 GHz. We used polymeric KC_{60} (Ref. 9) as a g-factor reference (g_{KC60} =2.0006) for the high-frequency measurements. We determined g_{KC60} by comparing it to Mn:MgO at 222.4 GHz (g_{Mn}=2.0009). We tested the most important results (splitting of ET and Mn^{2+} ESR lines, temperature, orientation, and frequency dependence of ESR resonance) on 2 or more crystals. Results of measurements on different crystals are similar.

III. STRUCTURE

$ET_2MnCu[N(CN)_2]_4$ has an unusual structure in which the ET radical cations are embedded in a 3D polymeric network of bimetallic dicyanamide $[dca=N(CN)_2]$ anions.[4] In simple salts, dca ligands bridging transition metal ions in the anion polymer are known to mediate magnetic interactions.[10] There are several short intermolecular contacts between the magnetic anion network and the organic radical cations.

The structure is monoclinic with β=96°. Octahedrally coordinated manganese ions connected by dca ligands form two-dimensional layers in the (b,c) plane of the crystal (Fig. 2). These layers are somewhat anisotropic: the lengths of the orthogonal b and c lattice vectors are 10.6 Å and 12.4 Å, respectively. The structure suggests a quasi-two-dimensional magnetic behavior since the distance between Mn^{2+} ions within the (b,c) plane (7.8 Å) is much less than the interplanar Mn-Mn distance, $a/2$=16 Å. There are two differently oriented Mn^{2+} environments. Layers of ET molecules alternate with the manganese layers. Linear $Cu[N(CN)_2]_2$ chains connect the 2D anionic layers along the a direction (through the ET layers) into a 3D network with a=31.9 Å. The four ET molecules surrounding a $Cu[N(CN)_2]_2$ bridge are crystallographically independent and the unit cell contains four formula units. Formally there is one hole per two ET molecules.

Resistivity measurements revealed a transition between two semiconducting phases (semiconductor I and II) at 292 K. X-ray measurements indicate a small structural change at this transition with a redistribution of the charge among ET molecules. The weak conductivity has been attributed to the ET layers.[4]

TABLE I. Crystallographic data and refined structural parameters for the $(ET)_2CuMn[N(CN)_2]_4$ salt. The crystal has a monoclinic space group, P21/n. The chemical formula of the material is $C_{28}H_{16}N_{12}S_{16}MnCu$ and there are four formula units in the unit cell.

Temperature (K)	123 K	280 K	330 K
F(000)	2312	2312	2312
μ(Mo-Kα), mm-1	1.673	1.643	1.629
a/Å	32.0699(16)	32.0575(19)	32.059(2)
b/Å	10.5282(6)	10.6643(6)	10.7160(7)
c/Å	12.3039(6)	12.3731(8)	12.4218(8)
β/°	95.953(4)	96.000(5)	96.255(5)
V/Å^3	4131.9(3)	4206.8(4)	4242.0(5)
2θ max/°	53.68	50.70	50.70
Number of unique reflections	8763	7664	7725
Number of independent reflections with $I \geq 2\sigma(I)$	7461	5795	5484
Number of refined parameters	543	542	542
R	0.0769	0.0523	0.0555
GOF		1.044	1.017

X-ray diffraction data were obtained at 330 and 280 K, above and below the phase transition and at 123 K. Crystallographic data are summarized in Tables I and II. These data confirm that the phase transition at 292 K is driven by a charge redistribution on the ET radical cations.

Figure 3 shows the central C=C bond lengths in the ET radical cations above and below the phase transition. The central C=C bond length in the ET molecule depends on the charge of the molecules.[11–13] The bond lengths change most near the phase transition. At 330 K the central C=C bond lengths correspond to the same 0.5 oxidation state[11] within experimental error in all the four different radical cations, designated by A, B, C, and D. Below the transition, radical cations A and C change little and their oxidation state remains 0.5. In radical cation B the bond length decreases to a value that is characteristic to the neutral ET molecule. In molecule D the central C=C bond length elongates and the oxidation state is approximately +1.[11,13] Probably, the charge redistribution on the ET radical cations is stimulated by their rearrangement (Table II). The anomalous, i.e., negative thermal expansion of the a lattice parameter shown by x-ray diffraction below the phase transition at 292 K hints at a structural modulation.[14]

TABLE II. Values of dihedral angles between the ET radical cations in the structure of the $(ET)_2CuMn[N(CN)_2]_4$ salt at different temperatures. Relative reorientation of molecule C is remarkable.

Value of the dihedral angle between the neighboring radical cations, °	123 K	280 K	330 K
A-B	67.7	68.6	68.4
B-D	46.6	46.2	46.0
D-C	83.0	84.2	81.1
C-A	62.0	61.8	59.0

IV. MAGNETIC MEASUREMENTS

A. Magnetic susceptibility

Previous static susceptibility measurements[4] in powder samples showed a simple paramagnetic behavior with weak antiferromagnetic correlations at low temperatures. The present SQUID magnetization measurements on single crystals along a^*, b, and c show that the susceptibility χ is almost isotropic. There is a slight anisotropy below 5 K where χ is 5% larger in the b direction than in the a^* and c directions.

The comparison of the magnetization versus magnetic-field curves with Brillouin functions agrees with an assumption that above 5 K magnetism arises from nearly free Mn^{2+} ions with $S=5/2$ spin and the $S=1/2$ spins formally carried by every second ET (Fig. 4). Since the mass of the sample

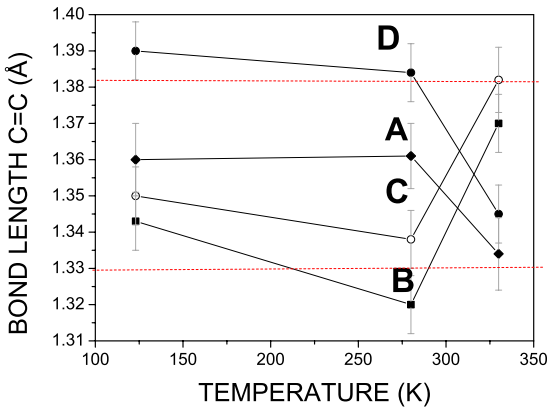

FIG. 3. (Color online) Temperature dependence of the central C=C bond lengths in the ET radical cations. A, B, C, and D denote crystallographically independent ET radical cations. Dotted lines mark the boundaries between regions corresponding to neutral, +1/2 and +1 oxidation states of the molecule, in order of increasing bond length.

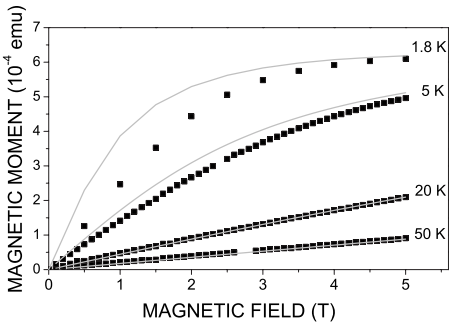

FIG. 4. Magnetic moment vs magnetic field along the *b* axis at several temperatures. Solid lines are sums of $S=5/2$ and $S=1/2$ Brillouin functions corresponding to free Mn^{2+} ions and ET molecules, respectively. The amplitude of the function was fitted to the 20 K data and there are no further fitting parameters in the curves.

could not be measured with high enough precision, we normalized the Brillouin function amplitude to the measurement at 20 K. At and below 5 K, the low-field magnetization is smaller than expected from the Brillouin function indicating antiferromagnetic correlations. We show in Sec. IV C 3 that the intralayer exchange interaction between Mn ions is actually quite strong but due to the two-dimensionality, this is not apparent in the static susceptibility.

B. Electron spin resonance at high temperatures

1. ESR active sites

The ESR spectrum consists of a single line at room temperature and 9.4 GHz. We measured the absolute intensity of the ESR spectrum using a spin $S=1/2$ reference, $CuSO_4 \cdot 5H_2O$. The mass of the sample was determined from its linear dimensions measured under a microscope. The measured molar susceptibility ratio of reference and sample, $\chi_{\text{sample}}/\chi_{\text{CuSO}_4}=10.4\pm3.3$ is close to 38/3, the value expected for free $S=5/2$ Mn^{2+} ions and $S=1/2$ spins on every second ET molecule. This proves that the ESR arises from all Mn fine structure transitions, which are motionally narrowed into a single line. ET molecules contribute also to the ESR as their line is resolved at high frequencies.

2. Resolved ESR of Mn and ET at high temperatures

For magnetic field *B* in the a^* direction, the resonances of the Mn^{2+} and ET spins are resolved at higher frequencies (315 and 420 GHz) and temperatures above 120 K (Fig. 5). In all measurements there is a single Mn line for the two Mn^{2+} ions in differently oriented $(CN)_6$ octahedra, thus Mn^{2+} ions within a molecular layer have a relatively large exchange. The same is true for the ET molecules. However, at high temperatures the overlap between Mn^{2+} and ET spins is small and their lines are resolved in high magnetic fields. The intensity ratio of the lines measured from Lorentzian fits proves that the smaller line comes from the ET molecules (Fig. 5).

The shifts of the two lines versus frequency at 300 K are plotted in Fig. 6. Below 210 GHz there is a common resonance at all temperatures. Taken the Mn ESR alone, the frequency dependence of the shift is nonlinear. However, the intensity-weighted average shift of the two lines is linear with frequency; this suggests that the Mn^{2+} and ET have exchange coupled resonances with slightly different *g* values. The condition for resolving narrow lines of closely spaced magnetic species with *g* factors, g_1 and g_2 is that the line separation is larger than the exchange energy

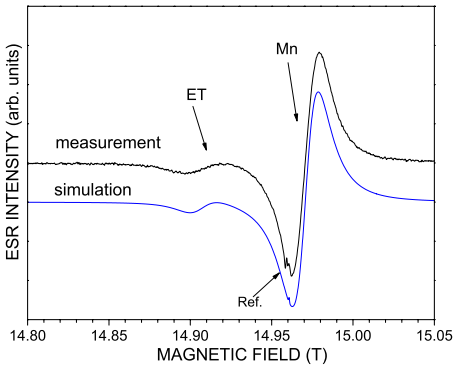

FIG. 5. (Color online) Upper curve: ESR spectrum in the a^* direction at 420 GHz and 300 K. Resolved lines correspond to the Mn^{2+} ions and the ET molecules. The small sharp signal at 14.96 T is the *g*-factor reference. Lower curve: simulation of the measured spectrum.

$$\Delta\varepsilon = (g_1 - g_2)\mu_B B > J. \quad (1)$$

We use this expression to estimate the exchange interaction between the spin species. We assume that at 420 GHz the splitting of the lines is little affected by the exchange and represents the *g*-factor splitting of the two magnetic species.[15] The measured splitting of 66 mT is thus equivalent to $\Delta g=0.009$. The splitting decreases at lower frequencies and cannot be resolved below 200 GHz, thus it approximately equals to the exchange interaction at this frequency. Based on these numbers the estimated exchange coupling is $|J_{\text{Mn-ET}}| \approx 0.04$ K. The sign, i.e., whether the coupling is fer-

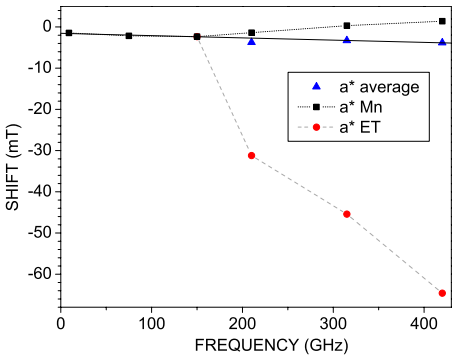

FIG. 6. (Color online) Shift of the ESR line with respect to the KC_{60} reference in the a^* direction at 300 K as a function of frequency, corrected for dipole fields, $\Delta B_a = \Delta B_a^{\text{meas}} - \Delta B_{\text{Ma}}$ (see Sec. IV C 1). The Mn and ET lines shift nonlinearly (solid squares and circles, respectively) but the average of the two resonances (triangles) is linear with frequency (solid line). The lines are guides to the eye.

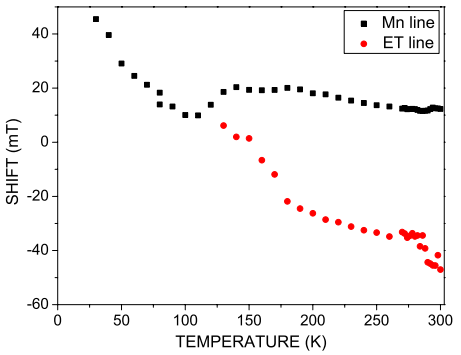

FIG. 7. (Color online) Shifts of the Mn and the ET ESR lines with respect to the KC_{60} reference as a function of temperature on cooling at 420 GHz in the a^* direction. The phase transition at 291 K is marked by a jump in the shift of the ET line. There is another broad transition between 180 and 120 K where the ET line shifts rapidly toward the Mn line.

romagnetic or antiferromagnetic could not be determined from the ESR spectra.

Although it is uncommon to detect separate resonances of spin species with $g \approx 2$ in dense magnetic systems, it is not unheard of among the layered ET compounds. Resolved resonances of conduction electrons and paramagnetic ions were detected in the organic metals β'' $-ET_4NH_4[Cr(C_2O_4)_3]\cdot DMF$ (Ref. 6) and $ET_3CuCl_4\cdot H_2O$ (Ref. 5).

Decreasing the temperature from 300 to 120 K, the Mn and ET lines shift toward each other and gradually merge into a single line (Fig. 7). On cooling, the two lines merge gradually below 180 K and cannot be resolved below 130 K (Fig. 7). The ESR spectra show a hysteresis with temperature cycling, but we have not studied this hysteresis systematically. We identify the merging of the lines as a phase transition between 180 and 120 K. The transition is probably related to the localization of spins in the ET layers and the anomalous temperature dependence of the lattice constants. Further measurements are required to better understand the nature of the transition.

The Mn and ET lines are not resolved in the (b,c) plane, presumably because the g factors of the spin species differ less in this plane than in the a^* direction. The width of the single line in the (b,c) plane has a quadratic frequency dependence above 75 GHz (Fig. 8). This quadratic frequency dependence may arise from the complete exchange narrowing of the g-factor split ET and Mn ESR lines. In the strong exchange limit, the width of the line is proportional to the square of the g-factor splitting.[16]

$$g\mu_B \Delta B \sim \frac{(\hbar\Delta\omega)^2}{J}, \tag{2}$$

thus at frequencies where the splitting is much larger than the exchange frequency $(\Delta\omega \gg J/\hbar)$, a linearly frequency dependent splitting appears, while at lower frequencies a single line with a quadratically frequency dependent width is observed.

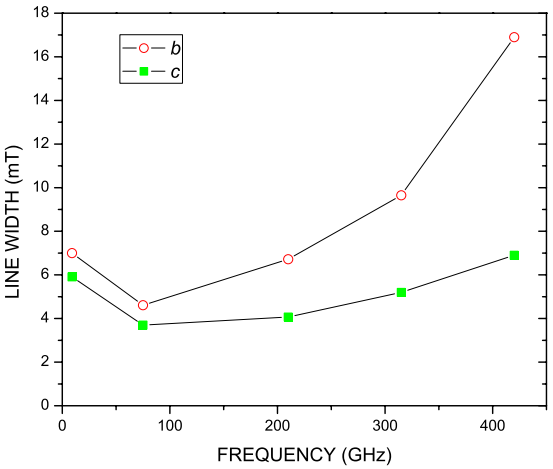

FIG. 8. (Color online) Frequency dependence of the line width along the b and c directions at 260 K. The line width shows a quadratic frequency dependence above 75 GHz.

Below 75 GHz a new line broadening mechanism appears. The line broadens by about 2.2 mT between 75 and 9.4 GHz in both in-plane directions at all temperatures from room temperature down to 100 K. At present we do not have a consistent explanation.

C. Determination of the low-temperature crystal fields

In contrast with the almost isotropic magnetization, there are large anisotropic ESR shifts at low temperatures (Fig. 9). The shifts are temperature dependent and saturate in a field

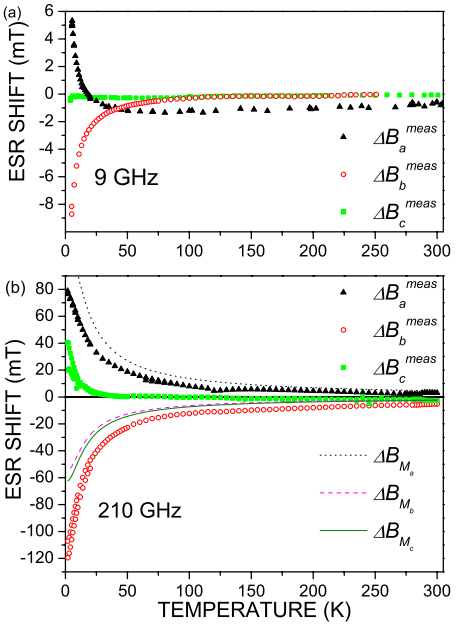

FIG. 9. (Color online) Temperature dependence of the resonance field (a) at 9 GHz and (b) at 210 GHz in the three principal directions. A large anisotropy is observed below 150 K. In panel (b) the calculated ESR shifts due to dipole-dipole interaction, $\Delta B_{Ma}(T), \Delta B_{Mb}(T)$ and $\Delta B_{Mc}(T)$, are indicated by dotted, dashed, and solid lines, respectively.

of 15 T and at 3 K at 80 mT, −120 mT and 40 mT in the a^*, b, and c directions, respectively. We attribute these shifts to dipolar fields and fine structure splitting. It is unusual that these interactions shift the line and not only broaden it. However in high magnetic fields at low temperatures, only the lower lying Zeeman levels are populated, following the Boltzmann distribution. The ESR is a motionally narrowed average of all transitions and it shifts toward the frequencies of the transitions between more populated levels.

At temperatures below about $k_BT<5\mu_BB_{\rm res}$ (where $B_{\rm res}$ is the resonance field) the line splits into several components in an uncontrolled way. Mechanical strains rendering the fine structure inhomogeneous are the likely reason for this splitting. We use the first moment of the spectrum to quantify the resonance field of these split lines.

1. Dipolar shifts

Dipolar interactions give rise at high fields and low temperatures to large anisotropic ESR shifts, which we calculate classically. In the first step, we calculate the local magnetic field at a Mn site as a function of Mn^{2+} magnetization and then we solve the equation of motion for the magnetization to find the resonance frequency. To determine the local field, the average demagnetizing field due to Mn^{2+} and ET spins was calculated approximating the shape of the sample with an infinite flat plate with demagnetizing factors $n_{xx}=n_{yy}=0$ and $n_{zz}=1$. (x, y, and z are orthogonal coordinates along c, b, and a^*, respectively). To take into account the anisotropic local environment, the average demagnetizing field was replaced in a spherical volume centered on an Mn site by the numerically calculated sum of the dipole fields of Mn^{2+} and ET spins.

We first calculated the local field at $T=0$ temperature with all moments aligned along the external field, $\underline{B}_0$

$$\underline{B}_{loc}=\underline{B}_0+\mu_0\underline{\underline{\alpha}}\underline{M}. \tag{3}$$

At $T=0$ the magnetization is $\mu_0M=66.9$ mT and $\alpha_{xx}=0.5978$, $\alpha_{yy}=0.5516$, $\alpha_{zz}=-1.1493$. Although the crystal is monoclinic, the tilt is small and the off-diagonal elements of the matrix α_{ij} are negligibly small ($\sim 10^{-2}$).

We obtain the ESR shifts from the magnetic free-energy density F

$$F=-\underline{M}\underline{B}-\frac{1}{2}\mu_0\underline{M}\,\underline{\underline{\alpha}}\,\underline{M} \tag{4}$$

and

$$\underline{M}\times(-\,\mathrm{grad}_M F)=\frac{1}{\gamma}\frac{d\underline{M}}{dt} \tag{5}$$

where γ is the gyromagnetic ratio and the g-factor anisotropy is neglected.

We solve the equation of motion for small perturbations around the equilibrium to obtain the resonance frequency $\omega/2\pi$, assuming $\mu_0M\ll B_0$. The zero temperature dipolar shift with the external field along the z axis is

$$\Delta B_{\rm Ma}=-\frac{\omega}{\gamma}+B_0=\frac{\mu_0M}{2}(\alpha_{yy}+\alpha_{xx}-2\alpha_{zz}). \tag{6}$$

There are similar expressions for the b and c directions. We find $\Delta B_{\rm Ma}=1.918\mu_0M$, $\Delta B_{\rm Mb}=-0.910\mu_0M$, and $\Delta B_{\rm Mc}=-1.007\mu_0M$.

We extended the calculation to finite temperatures by assuming that the temperature dependence of the magnetization $M(T)$, follows that of the sum of noninteracting Mn^{2+} and ET spins. This is a good approximation from room temperature to 25 K, where the measured susceptibility is paramagnetic and the ratio of the two Brillouin functions is quasi-constant. The ESR dipolar shifts $\Delta B_{\rm Ma}(T)$, $\Delta B_{\rm Mb}(T)$, and $\Delta B_{\rm Mc}(T)$, calculated by replacing M with $M(T)$ in Eq. (6), are plotted in Fig. 9. Although dipolar shifts are large, they clearly do not explain the observed anisotropy at low temperatures.

In the following we discuss the origin of the large anisotropic shifts remaining after the measured ESR shifts $\Delta B_i^{\rm meas}(T)$ (with respect to the KC_{60} reference) are corrected for the calculated dipolar shifts. [$\Delta B_i(T)=\Delta B_i^{\rm meas}(T)$-$\Delta B_{{\rm M}i}(T)$, $i=a^*$, b, and c]. These remaining shifts are negative and of similar magnitude along the a^* and b directions and positive and approximately twice as large along the c direction. At 210 GHz the saturated $\Delta B_i(T\to 0)$ values are −58 mT, −56 mT and 99 mT for $i=a^*$, b and c, respectively.

2. Two-dimensional correlations

Anisotropic ESR shifts in low-dimensional antiferromagnetic spin systems were studied by Nagata *et al.*[17,18] who explained their experimental observations by the combined effect of antiferromagnetic correlations and the dipole-dipole interaction. They derived an expression that relates the anisotropy of the ESR to the magnetic susceptibility. (Sample shape dependent demagnetizing effects were subtracted separately.) Uniaxial single ion anisotropy was taken into account up to second order, but only with a special orientation perpendicular to the 2D structure.

In our case the measured shifts, corrected for sample shape dependent demagnetizing effects, but not for local dipole fields are 3.4, −83, and 65 mT along the a^*, b, and c directions, respectively. The predictions of Nagata's model, due to its assumption of uniaxial symmetry of all interactions would be of the form $\Delta_{a^*}/2=-\Delta_b=-\Delta_c$ in contradiction with our observation of an anisotropy in the (b,c) plane. Thus, the Nagata model cannot describe the dominant source of the observed low-temperature shifts.

3. Motionally narrowed fine structure

We propose that the large low temperature anisotropy in $\Delta B_i(T)$, the ESR resonance shift corrected for dipolar shifts, arises from the single ion anisotropy of Mn^{2+} ions. A magnetic ion in a crystal interacts with the electrical charges of its environment, the so called crystal field. As a result, for spins greater than $\frac{1}{2}$, the fine structure lines split, which can be described by the so called zero-field splitting (ZFS) parameters in the corresponding spin Hamiltonian. In dilute

magnetic systems the ZFS parameters are usually derived from the magnetic-field orientation dependence of the fine structure lines. In magnetically dense systems, the fine structure is not resolved and only few studies go beyond a qualitative description.[19]

Here we determine the ZFS parameters of Mn^{2+} ions to second order in the spin operators from the temperature dependence of the single exchange-narrowed line. In our simplified model, we assume that the fine structure merges into a single resonance line as a consequence of exchange narrowing. A similar model was used previously for dilute alloys.[19] The spin Hamiltonian of the Mn^{2+} ion is:

$$H = H_Z + H_{ZFS} + H_{EX} = \sum_j \left(g\mu_B \underline{B} \underline{S}_j + \frac{1}{3} b_{20} O_2^0(j) + \frac{1}{3} b_{22} O_2^2(j) \right) + \frac{1}{2} \sum_{\langle j,k \rangle} J_{\text{Mn-Mn}} \underline{S}_j \underline{S}_k. \quad (7)$$

Here $\underline{B}$ is the local magnetic field at the Mn site, $\underline{S}_j$ is the Mn^{2+} spin vector operator at site j, and we neglected the anisotropy of the g factor. The average ZFS of the Mn^{2+} ions in the two different distorted $(CN)_6$ octahedra is parameterized by b_{20} and b_{22}. $O_2^0(j) = 3S_{jz}^2 - S(S+1)$ and $O_2^2(j) = S_{jx}^2 - S_{jy}^2$ are second order Stevens operators at site j and the fourth order terms are omitted. $J_{\text{Mn-Mn}}$ is the average isotropic exchange energy. The x, y, and z axes are along c, b, and a^*, respectively. The shifts arise from the temperature-dependent populations of the energy levels.

Figure 10 illustrates the way the model leads to anisotropic shifts that are in good agreement with the observations. The Zeeman term, H_Z, splits the magnetic levels of the free Mn^{2+} ion into six equally spaced energy levels. The ZFS term, H_{ZFS}, shifts the Zeeman levels unevenly and without H_{EX} it would give rise to the ESR fine structure of an isolated Mn^{2+} ion embedded in the $(CN)_6$ octahedron [Fig. 10(b)]. The relative intensities of these lines change at low temperatures and high magnetic fields ($g\mu_B B > \approx k_B T$) as the higher lying levels depopulate following the Boltzmann distribution. At very low temperatures and high magnetic fields, only the lowest lying $-5/2$ level is populated and all intensity shifts to the $-5/2 \rightarrow -3/2$ transition. The exchange term H_{EX}, is a true many-body term, which we treat qualitatively by assuming that the observed single line appears at the intensity-weighted average resonance field of the fine structure lines. Incomplete exchange narrowing of the fine structure is well known to contribute to the ESR line width.[16] At the low temperatures and high fields of the experiments changes in the thermal population of the energy levels shift the resonance significantly.

We suppose crystal fields are temperature independent below 120 K and calculate the ZFS parameters from the measured anisotropic shifts at 210, 315, and 420 GHz and at temperatures 2 and 110 K. We find the ZFS parameters $b_{20} \approx -340$ MHz and $b_{22} \approx 1057$ MHz. The temperature dependence of the calculated shift is shown in Fig. 10(a) for $B \| b$ and results are similar in the other two directions. The above second-order parameters indicate that the local environment

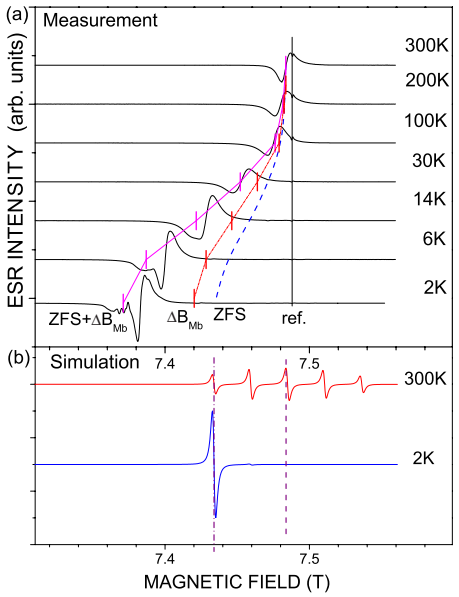

FIG. 10. (Color online) (a) Shift of the ESR for $B \| b$ at 210 GHz. Vertical solid line (ref.): KC_{60} reference; dashed line (ZFS): shift calculated from exchange-narrowed zero-field splitting; dash dotted line (ΔB_{Mb}): shift from dipolar fields; solid line (ZFS $+\Delta B_{\text{Mb}}$): sum of the shifts from unresolved ZFS and dipolar fields. (b) Simulation of the spectrum of an isolated spin with ZFS at two temperatures. The intensities of the transitions depend on the population of the Zeeman levels and change with temperature. Dashed and dotted lines indicate the intensity-weighted average of the resonance field at 300 and 2 K, respectively. (ZFS parameters: $b_{20} = -340$ MHz, $b_{22} = 1057$ MHz. Relative amplitudes of the spectra are arbitrary.)

is strongly distorted from cubic symmetry along the c axis. This is different from the structure expected from x-ray measurements at ambient temperatures, which suggests that the distortion is largest along a^* and the anisotropy within the (b,c) plane is smaller. X-ray measurements below 100 K, well below the broad phase transition about 150 K could directly verify our model.

We estimate the exchange interaction $J_{\text{Mn-Mn}}$ from the measured $\Delta\omega$ line width and the ω_p "breadth" of the fine structure, i.e., the distance between the outermost fine structure lines that would appear in the absence of Mn–Mn exchange. An approximation[20] valid for a 2D system is

$$\Delta\omega = \frac{\omega_p^2}{J_{\text{Mn-Mn}}/\hbar} \ln\left(\frac{J_{\text{Mn-Mn}}/\hbar}{\omega_p} \right). \quad (8)$$

The logarithmic term is specific to the 2D nature of the Mn layers; the exchange interaction is less effective in narrowing the lines in a 2D than in a 3D system.[21] The width of the fine structure in the c direction is $\omega_p \approx \gamma \cdot 0.2$ T. Using $\Delta\omega = \gamma \cdot 5.7$ mT, a value extrapolated from high field data to zero field at 100 K, where the line is the narrowest and is weakly affected by strains or other inhomogeneous terms, we find $J_{\text{Mn-Mn}} \approx -48$ K. The coupling is antiferromagnetic ($J < 0$) which we deduce from static susceptibility measurements at low temperature. The interaction between the manganese planes is much smaller, as antiferromagnetic correlations

emerge only below 20 K and there is no sign of a static magnetic order down to 1.2 K.

In principle, ESR also gives information on the fine structure at high temperatures. The resonance is shifted at low frequencies when the ZFS is comparable to or larger than the Zeeman splitting. Shifts at temperatures above 100 K which are not proportional to the frequency between 9.4 and 75 GHz, (Fig. 9), may have this origin.

V. CONCLUSIONS

We investigated the structural and magnetic properties of $ET_2MnCu[N(CN)_2]_4$, an organic paramagnetic compound with an unusual three-dimensional anionic network. Although the static susceptibility is apparently well described by noninteracting spins above 5 K with only weak antiferromagnetic correlations below, the detailed analysis of the ESR spectra reveal a more complex picture.

The system is composed of weakly interacting magnetic planes, but there is considerable exchange interaction within the 2D subsystems. We estimate an exchange coupling among the manganese ions in the (b,c) plane, $J_{\text{Mn-Mn}} \approx -48$ K, using the line width and the ZFS parameters obtained from the low-temperature shifts. On the other hand, the coupling between the different spin species is so small that their resonances are resolved above 120 K in spite of the similar g values. We estimate an exchange coupling at 300 K of $|J_{\text{Mn-ET}}| \approx 4 \cdot 10^{-2}$ K.

We detected a first-order phase transition between 180 and 120 K, which shows a hysteresis with thermal cycling. The anomalous temperature dependence of the a lattice parameter suggests that a structural modulation develops along the a direction below 292 K. It is plausible that the structural anomaly relates to the phase transition observed in the ESR. More measurements are needed to understand the transition. Preliminary ESR results indicate that x-ray measurements below 120 K could be conclusive.

Static magnetization is almost isotropic at all temperatures while significant ESR shifts were detected below 140 K. We described the spectra quantitatively, assuming a considerable zero-field splitting of the manganese ESR corresponding to a strong distortion of the $Mn(CN)_6$ octahedra in the (b,c) plane. The exchange interaction merges the Mn^{2+} fine structure into a single line, however, it gives rise to anisotropic shifts and the most important ZFS parameters are measurable at low temperature and high magnetic fields.

ACKNOWLEDGMENT

This work was supported by Hungarian State Grants (OTKA) No. PF63954, K68807, NK60984, and NN76727 by the Swiss NSF and its NCCR "MaNEP" and by RFBR-DFG project No. 07-02-91562 (RUS 113/926/0-1). T.F. acknowledges support from the János Bolyai program of the Hungarian Academy of Sciences. B.N. acknowledges support from the Prospective Researcher program No. PBELP2-125427 of the Swiss NSF.

*kalmanagy@gmail.com

[1] E. Coronado and P. Day, Chem. Rev. **104**, 5419 (2004).
[2] C. Hotta, J. Phys. Soc. Jpn. **72**, 840 (2003).
[3] E. Coronado, J. R. Galán-Mascarós, C. J. Gómez-Garcia, and V. Laukhin, Nature (London) **408**, 447 (2000).
[4] N. D. Kushch, A. V. Kazakova, A. D. Dubrovskii, G. V. Shilov, L. I. Buravov, R. B. Morgunov, E. V. Kurganova, Y. Tanimoto, and E. B. Yagubskii, J. Mater. Chem. **17**, 4407 (2007).
[5] P. Day, M. Kurmoo, T. Mallah, I. R. Marsden, R. H. Friend, F. L. Pratt, W. Hayes, D. Chasseau, J. Gaultier, G. Bravic, and L. Ducasse, J. Am. Chem. Soc. **114**, 10722 (1992).
[6] R. B. Morgunov, R. P. Shibaeva, É. B. Yagubskii, T. Kato, and Y. Tanimoto, J. Exp. Theor. Phys. **102**, 121 (2006).
[7] G. M. Sheldrick, *SHELXS-97, Program for Crystal Structure Determination* (University of Gottingen, Germany, 1997).
[8] G. M. Sheldrick, *SHELXL-97, Program for the Refinement of Crystal Structure* (University of Gottingen, Germany, 1997).
[9] S. Pekker, L. Forró, L. Mihály, and A. Jánossy, Solid State Commun. **90**, 349 (1994).
[10] J. L. Manson, C. D. Incarvito, A. L. Rheingold, and J. S. Miller, J. Chem. Soc., Dalton Trans. **1998**, 3705.
[11] J. M. Williams, H. H. Wang, T. E. Emge, U. Geiser, M. A. Beno, P. C. W. Leung, K. D. Carlson, R. J. Torn, A. J. Shultz, and M.-H. Whangbo, *Progress in Inorganic Chemistry* (Wiley, New York, 1987) Vol. 35, p. 51–218.
[12] P. Guionneau, C. J. Kepert, G. Bravic, D. Chasseau, M. R. Truter, M. Kurmo, and P. Day, Synth. Met. **86**, 1973 (1997).
[13] V. E. Korotkov and R. P. Shibaeva, Sov. Phys. Crystallogr. **34**, 865 (1989).
[14] H. Negishi, Y. Kuroiwa, H. Akamine, S. Aoyagi, A. Sawada, T. Shobu, S. Negishi, and M. Sasaki, Solid State Commun. **125**, 45 (2003).
[15] P. W. Anderson, J. Phys. Soc. Jpn. **9**, 316 (1954).
[16] P. W. Anderson and P. R. Weiss, Rev. Mod. Phys. **25**, 269 (1953).
[17] K. Nagata and Y. Tazuke, J. Phys. Soc. Jpn. **32**, 337 (1972).
[18] K. Nagata, I. Yamamoto, H. Takano, and Y. Yokozawa, J. Phys. Soc. Jpn. **43**, 857 (1977).
[19] L. J. Tao, D. Davidov, R. Orbach, D. Shaltiel, and C. R. Burr, Phys. Rev. Lett. **26**, 1438 (1971).
[20] M. J. Hennessy, C. D. McElwee, and P. M. Richards, Phys. Rev. B **7**, 930 (1973).
[21] P. M. Richards and M. B. Salamon, Phys. Rev. B **9**, 32 (1974).